

InAs avalanche photodiodes as X-ray detectors

This content has been downloaded from IOPscience. Please scroll down to see the full text.

2015 JINST 10 P10030

(<http://iopscience.iop.org/1748-0221/10/10/P10030>)

View [the table of contents for this issue](#), or go to the [journal homepage](#) for more

Download details:

IP Address: 143.167.32.77

This content was downloaded on 04/12/2015 at 13:50

Please note that [terms and conditions apply](#).

InAs avalanche photodiodes as X-ray detectors

X. Meng,^a X. Zhou,^a S. Zhang,^a J. Lees,^b C.H. Tan^a and J.S. Ng^{a,1}

^aDepartment of Electronic & Electrical Engineering, University of Sheffield,
Mappin Street, Sheffield, S1 3JD, U.K.

^bSpace Research Centre, Department of Physics and Astronomy, University of Leicester,
Leicester, LE1 7RH, U.K.

E-mail: j.s.ng@sheffield.ac.uk

ABSTRACT: We designed and demonstrated an InAs avalanche photodiode (APD) for X-ray detection, combining narrow band gap semiconductor materials and avalanche gain from APDs. The InAs APD (cooled by liquid nitrogen) was tested with a ⁵⁵Fe X-ray source. Full width at half maximum (FWHM) from the spectra decreases rapidly with reverse bias, rising again for higher voltages, resulting in a minimum FWHM value of 401eV at 5.9 keV. This minimum value was achieved at 10 V reverse bias, which corresponds to an avalanche gain of 11. The dependence of FWHM on reverse bias observed is explained by the competition between various factors, such as leakage current, capacitance and avalanche gain from the APD, as well as measurement system noise. The minimum FWHM achieved is largely dominated by the measurement system noise and APD leakage current.

KEYWORDS: Solid state detectors; Charge transport and multiplication in solid media; X-ray detectors

¹Corresponding author.



Contents

1	Introduction	1
2	Device structure and electrical characteristics	2
3	X-ray response	3
4	Noise analysis	6
5	Conclusions	7

1 Introduction

Measurement of X-ray fluorescence with Si detectors is an established technique to perform elemental analysis in a wide range of applications, such as treatments of liquid hazardous wastes [1], environmental analysis of water and soil samples [2], in vivo tests on human patients [3], and food safety assessments [4]. The elements of interest often include heavy metals, such as Hg and Pb, requiring X-ray photon detection up to 80 keV. On the other hand, some toxic elements, such as Li and Be, emit X-rays that are < 100 eV in energy.

Although Si is the dominant material used to make soft X-ray detectors, the energy resolution of current commercial Si X-ray detectors is approaching its Fano limit. For example, an Amptek Si drift detector has an energy resolution of 125 eV at 5.9 keV [5], while Fano-limited energy resolution is 118 eV (calculated assuming 3.65 eV electron-hole-pair creation energy and 0.117 Fano factor [6]). Moreover, Si has a relatively small atomic number and crystal density, limiting its absorption coefficient at high X-ray energies. Thus alternative semiconductor materials to achieve low Fano-limited energy resolution and high absorption efficiency are desirable.

These criteria are met by certain compound semiconductors with narrow band gaps, E_g , such as InSb ($E_g = 0.165$ eV) and InAs ($E_g = 0.356$ eV [7]). They have relatively high atomic numbers (49/51 for InSb and 49/33 for InAs) and densities (5.78 g/cm³ for InSb and 5.68 g/cm³ for InAs [8]). Some progress has been made in using these narrow band gap materials for X-ray detectors.

InSb Schottky diodes fabricated from epitaxially grown crystals had been studied as radiation detectors [9–11]. Cooling the Schottky diode to 42 K, alpha particles (5.5 MeV in energy) were detected with 1.8 % FWHM [11]. These diodes also detected Gamma rays (59.5 keV in energy), however the gamma ray peaks were not resolved, due to noise caused by the extremely high detector's leakage currents even at cryogenic temperatures [9, 10]. In addition, in order to minimise the leakage current, the detectors were operated without bias, causing undesirably narrow depletion region and hence low collection efficiency. In another work, Zn diffusion was employed to fabricate InAs p-n diodes, which detected alpha particles when cooled by liquid nitrogen, but again high detector's leakage currents prohibited energy resolution assessment [12].

Si APDs have been extensively investigated for X-ray detection and demonstrated energy resolution of 360 eV at 5.9 keV at -20°C [13]. There are also reports of APDs made with a wide bandgap material, $\text{Al}_{0.8}\text{Ga}_{0.2}\text{As}$, showing promising results at room temperature (or elevated temperatures) [14, 15]. The improvement in SNR is brought by the APD's avalanche gain, M , when the signal is weak and/or the amplifier's noise is dominant. Both conditions apply to soft X-ray detection applications, where fewer electron-hole pairs are created by each photon compared to X-rays with higher energies. Having an appreciable M may improve the FWHM of the detected peak, with very little negative effect from the associated avalanche noise (often known as excess noise), if the APD is appropriately designed [16]. Appropriate designs need to be guided by the impact ionization properties of the semiconductor materials used. As an example, consider an avalanche material with electron ionization coefficient larger than hole ionization coefficient, $\alpha > \beta$, i.e. electrons yield higher gain than holes. Then the X-ray photons need to enter the APD from its p-layer, so that the majority of photo-generated carriers initiating the avalanche gain are electrons, rather than holes. This will ensure that the avalanche gain applicable to the photo-generated carriers is as high as practically possible.

We previously reported an InAs APD with an n-i-p structure for X-ray detection [17]. When cooled to 77 K, FWHM of the 5.9 keV peak reduced from 2.02 keV to 950 eV, as M increased from 1.58 to 5.3. This represented a significant progress in semiconductor APDs made with narrow bandgap materials for X-ray detection, given that other works on InSb and InAs X-ray detectors were and are still hindered by leakage currents. However, since $\alpha > \beta$ in InAs, an InAs APD requires a p-i-n structure to maximise the value of M experienced by the absorbed X-ray photons for a given reverse bias. Furthermore, the n-i-p structure led to considerable absorption in the n-layer and avalanche layer, degrading the peak-to-background ratio in the X-ray spectra [17]. Thus appropriate changes to InAs APD designs can bring further improvements in their X-ray detection performance. In this paper, we report the soft X-ray detection performance of InAs APDs with p-i-n structure.

2 Device structure and electrical characteristics

The InAs APDs were fabricated from an InAs p-i-n diode wafer grown on a 2" n-type InAs substrate by molecular beam epitaxy. Be and Si were used as the p- and n-type dopants respectively. The wafer structure, shown schematically in figure 1(a), consisted of a 300 nm p-layer, a $3.5\ \mu\text{m}$ InAs layer with graded p-doping, a $6.0\ \mu\text{m}$ InAs i-layer and a $1.0\ \mu\text{m}$ InAs n-layer. The $3.5\ \mu\text{m}$ InAs layer had doping grading (light to heavy from bottom to top) to help improve collection of minority electrons originally generated by X-ray photon absorption within the p-layer. In addition, a very thin $\text{AlAs}_{0.16}\text{Sb}_{0.84}$ p^+ -layer was included to reduce diffusion of electrons from the p-contact into the graded, reducing the bulk leakage current.

Standard photolithography and wet chemical etching were used to create circular mesa diodes from the wafer. Ti/Au (20/200 nm) were deposited to form p- and n- contacts for the diodes. The main wet chemical etchant used was a mixture of phosphoric acid, hydrogen peroxide and de-ionized water (ratio of 1:1:1). The main mesa etching was followed by finishing etches using a solution of sulphuric acid, hydrogen peroxide and de-ionized water (ratio of 1:8:80) [18], and diluted hydrofluoric acid. Sidewalls of the mesas were then passivated with negative photoresist

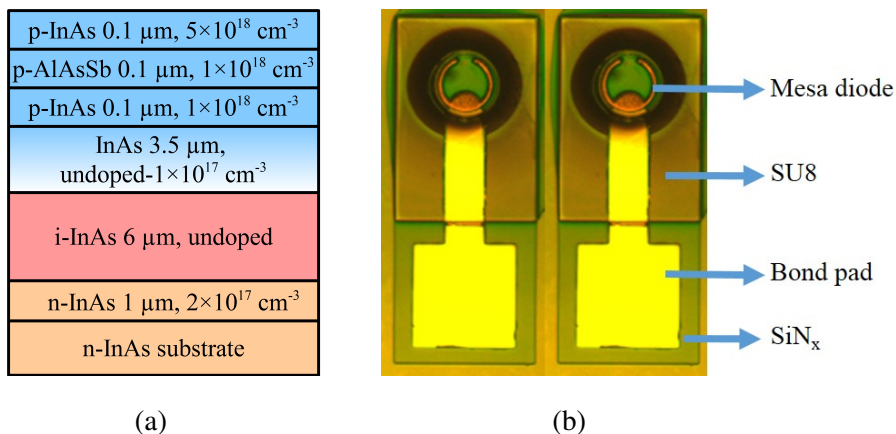


Figure 1. (a) Wafer structure of the InAs APD, showing the thickness and doping concentration for each layer. (b) Photograph of the mesa APD and its bond pad.

SU8, minimizing surface leakage currents degradation [19]. SiN_x was then deposited before the final step of bond pad deposition. The device fabrication yielded diodes with diameters ranging from 15 to 200 μm . The 75 μm diameter diodes, whose top view is shown in figure 1(b), offered the best trade-off between minimizing capacitance and maximizing the sensitive area for X-ray detection. Hence X-ray data presented later were obtained from diodes with 75 μm diameter, which were wire-bonded onto TO-5 packages to facilitate low temperature X-ray measurements.

The vast majority of the characterizations were carried out on two packaged InAs APDs, namely D1 and D2. Prior to X-ray measurements, reverse leakage currents of D1 and D2 were measured at room temperature, as shown in figure 2(a). At room temperature, due to the narrow band gap of InAs, the diodes' reverse leakage currents are prohibitively high. Comparison with on-wafer measurement data also indicates degradation in leakage currents caused by the packaging process. Cooling the device to 77 K reduces the bulk leakage current significantly [19], also shown in figure 2(a), making the detection of X-rays possible. On-wafer Capacitance-Voltage dependence of the 75 μm diameter InAs APD at 77 K, plotted in figure 2(b), shows that the capacitance decreased rapidly with reverse bias voltage from zero to 4 V, but remains relatively unchanged for higher reverse bias (0.18 pF at 10 V).

3 X-ray response

In the X-ray measurement setup, a TO-5 package containing the InAs APD was mounted onto the cold plate of a liquid nitrogen dewar to cool the APD down to ~ 77 K. A ^{55}Fe radioisotope with ~ 40 MBq activity was the irradiation source. Signal pulses from the APD were amplified by a charge-sensitive preamplifier (Amptek A250CF), before being shaped by a shaping amplifier (Ortec 570), which was in turn connected to a multichannel analyzer (MCA) controlled by a computer. Spectra obtained with different shaping time constants were compared, as shown in figure 3. Shaping time constant of 0.5 μs gave the narrowest peak so was selected for subsequent X-ray measurements. The acquisition time was 360 seconds for all measurements.

Figure 4(a) shows the ^{55}Fe spectra collected using the cooled APD D2, reverse biased at different voltages. The 5.9 keV energy peaks can be observed in all spectra. The peak position

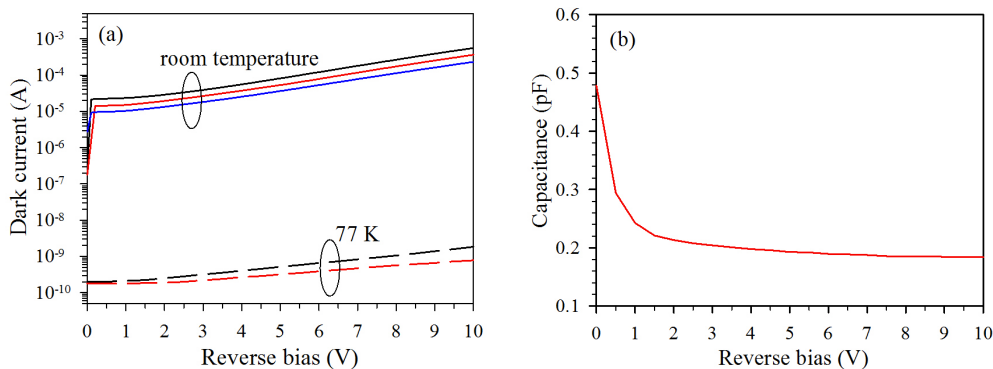


Figure 2. (a) Reverse leakage current of packaged InAs APDs with 75 μm diameter at room temperature (solid lines) and 77 K (dashed lines). At room temperature, data from TO-5 packages (black for APD D1 and red for APD D2) are higher than those from on-wafer measurements (blue line). (b) Capacitance-Voltage curve from on-wafer measurements at 77 K.

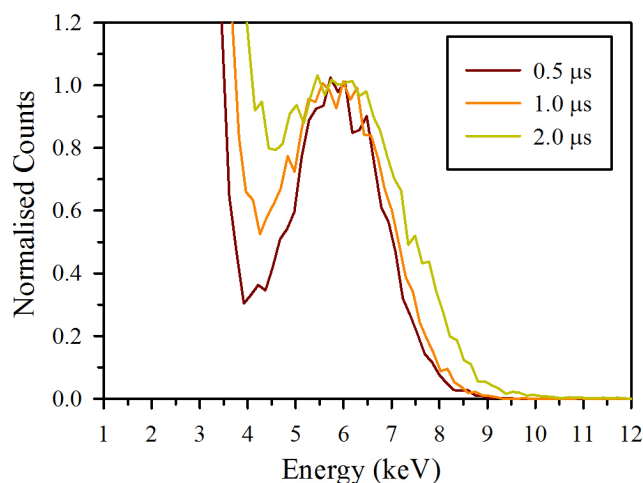


Figure 3. Energy spectra collected using APD D2 with different shaping time constants.

at a bias voltage of 0.4 V (channel 50) was assigned as the unity gain peak, because the peak position did not vary from 0 to 0.6 V reverse bias (data not shown here). As reverse bias voltage is increased beyond 0.6 V, the energy peak shifts to higher channel number, moving away from the noise peak, which is expected for an APD. Inset of figure 4(a) shows the unity gain peaks (channel 50) in the spectra at 3.0, 4.0 and 6.0 V reverse bias voltages. As reverse bias voltage increases beyond 6 V, it is increasingly difficult to resolve the unity gain peak from the growing noise peak (attributed to increasing leakage current shown in figure 2(a)).

For spectra at reverse bias voltages of 3.0, 4.0 and 6.0 V, the peak at channel 50 can be attributed to the fraction of incident X-ray photons absorbed in the InAs n-layer. These correspond to pure hole injection and the charge would experience an avalanche gain of M_h . For InAs APDs, M_h remains at unity for the entire range of reverse bias considered for this work [18]. Thus these unity gain peaks are expected to be present in the spectra for all reverse bias voltages. X-rays absorbed solely in the InAs p-layer will undergo a gain of M_e , which gives rise to the shifted main

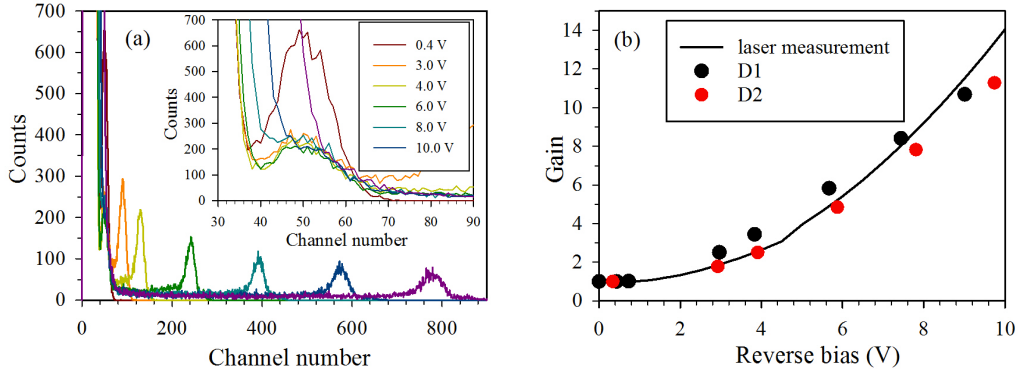


Figure 4. (a) Spectra in channel numbers collected using APD D2 cooled to 77K, at reverse bias voltages from 0.4 to 10.0 V. Inset: same data from channels 30 to 90. (b) Avalanche gain obtained from X-ray spectra of the InAs APDs at 77 K, in agreement with that from 1550 nm laser measurements.

peak. Absorption of X-ray photons within the InAs i-layer will give rise to an avalanche gain of M_{mix} , whose values range between unity and M_e , which accounts for the majority of the events between the M_h and M_e peaks, figure 4. Photon absorption in this region is clearly undesirable since it widens the main M_e peak, degrading the energy resolution.

Ratio of the channel number of shifted peaks to the unity gain channel number (50) gives M_e as a function of reverse bias, as shown in figure 4(b). The results are compared to M_e data obtained using conventional photomultiplication measurements (photocurrent measurement with a 1550 nm laser as photon source) on a device from the same sample. The two sets of data are in agreement, confirming that the shifted peaks were indeed due to avalanche gain.

The spectra shown in figure 4(a) have noise peaks with centroid at channel number 11 (not shown here) due to an offset of the MCA. With the noise peak (channel number 11) and 5.9 keV peak (channel number varies due to varying M_e) as references, the spectra in figure 4(a) were also converted from channel numbers into energy. The resultant normalized spectra for different reverse bias voltages are compared in figure 5. As reverse bias voltage increase, the energy peak becomes narrower, with better energy resolution. Meanwhile, the influence of noise tail is diminishing due to the positive effect of avalanche gain, achieving an overall increased signal to noise ratio.

Gaussian fitting to data in figure 5 yields FWHM values for the 5.9 keV peaks in each spectra. The deduced FWHM versus reverse bias of the InAs APDs is shown in figure 6. For APD D1, FWHM reduces from 2.12 keV at 0.5 V to a minimum of 660 eV at 6 V. APD D2 exhibits even smaller FWHM, a minimum of 401 eV at 10 V, which is significantly smaller than the value of 950 eV from ref. [17]. The decreasing FWHM with reverse bias observed from figure 6 is attributed to increasing M that reduces the effect of electronic noise, which is one of the dominant noise sources at small reverse bias. Reduction in FWHM with reverse bias is less significant at higher reverse bias, or even reversed in the case of APD D1, which is most likely caused by the increasing APD dark current, which grew in significance as a noise source (as seen in figure 2(a) and discussed in section 4). The better energy resolution of APD D2 (compared to APD D1) is attributed to its lower leakage current at the operating temperature, as shown in figure 2(a).

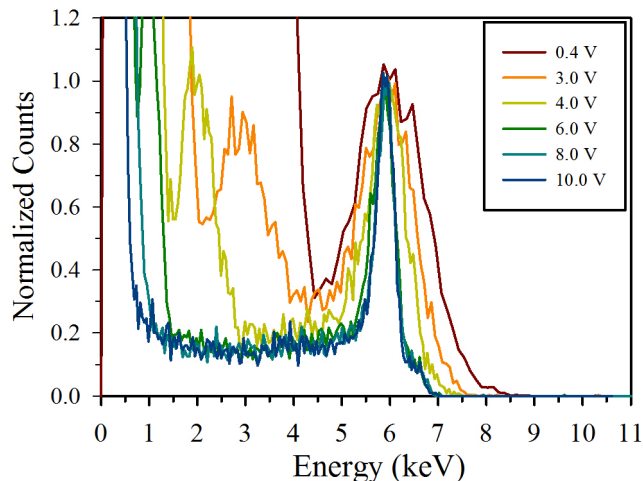


Figure 5. Energy spectra collected using the APD D2 cooled to 77 K, at reverse bias voltages from 0.4 to 10.0 V.

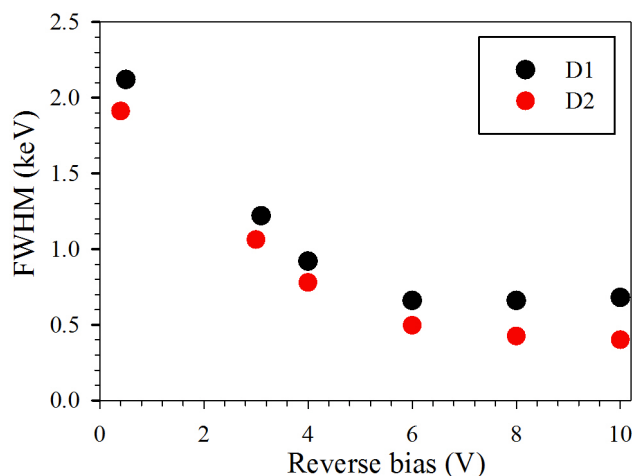


Figure 6. Energy resolution (FWHM) versus reverse bias from ^{55}Fe spectra measured with APDs D1 and D2.

4 Noise analysis

To assess in detail the significance of electronic noise to the measured energy resolution, measurements were conducted to assess the noise of the X-ray detection experimental setup used. To facilitate the noise measurements, a few modifications were made to the setup. The X-ray source was absent and square wave signals (from a pulse generator) were fed into a test capacitor (0.5 pF) within the preamplifier. The InAs APD (D2) remained connected to the input of the preamplifier, so that the noise contributions from detector leakage current and capacitance were included in the noise measurements. The preamplifier, shaping amplifier and MCA settings as for section 3 were used. Data were also taken without the detector.

The spectra obtained with or without D2 at different reverse biases are compared in figure 7 (plotted in channel numbers). Unsurprisingly, it shows peaks widened with reverse bias (beyond

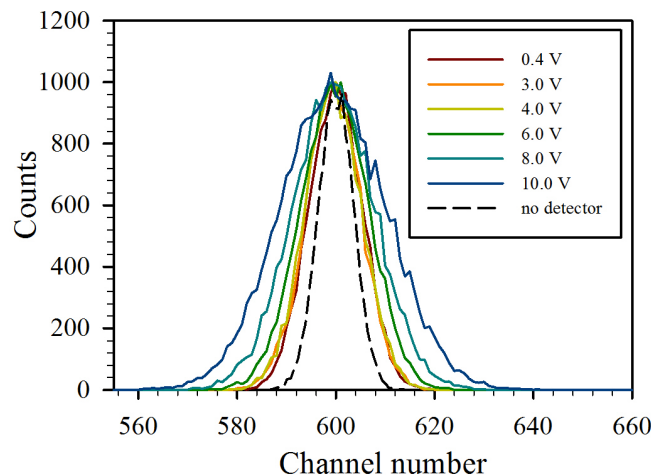


Figure 7. Spectra in channel number from noise measurements obtained with D2 at different reverse biases. Noise spectrum taken without the detector is also shown. The same width were obtained when different signal amplitudes from the pulse generator were used.

4.0 V), since leakage current continued to increase but capacitance remained relatively constant beyond 4.0 V. Noise spectrum obtained with D2 biased at 0.4 V was then converted into energy using identical references as for the 0.4 V X-ray data in figure 5. At 0.4 V reverse bias (no avalanche gain), the FWHM values from the X-ray peak (1.91 keV) and the noise measurements (1.89 keV) differ slightly, probably caused by fluctuations in the number of electron-hole pair created and incomplete collection of carriers created by photon absorption in the partially depleted InAs i-layer. FWHM of the noise peak obtained without the detector was 1.09 keV, which is high and increases when detector is connected. Nevertheless, the APD's avalanche gain works to significantly reduce the detrimental effect of electronics noise, achieving an overall energy resolution of 401 eV.

5 Conclusions

Using InAs APDs with a p-i-n structure, we obtained an energy resolution as small as 401 eV FWHM at 5.9 keV (with an avalanche gain of 11), significantly smaller than previously reported value (950 eV) from an InAs APD with an n-i-p structure. The improvement demonstrates the benefits provided by the combination of using InAs to absorb X-ray photons and adopting appropriate APD design. The energy resolution achieved in this work is largely limited by the APD leakage current and measurement system noise. Hence further improvement on the InAs APD X-ray performance requires efforts, in addition to more APD-specific modifications such as minimizing X-ray photon absorption within the InAs avalanche layer.

Acknowledgments

This work was supported by the U.K. Engineering and Physical Sciences Council (EPSRC) under grants EP/I010920/1 and EP/K001469/1. The work of J.S. Ng was supported by Royal Society University Research Fellowship.

References

- [1] A. Russell and R. James, *Determination of toxic elements in liquid hazardous waste using high-resolution energy-dispersive X-ray fluorescence spectrometry*, *J. Analy. Atom. Spect.* **12** (1997) 25.
- [2] F.L. Melquiades and C.R. Appoloni, *Application of XRF and field portable XRF for environmental analysis*, *J. Rad. Nucl. Chem.* **262** (2004) 533.
- [3] J. Borjesson and S. Mattsson, *Medical applications of X-ray fluorescence for trace element research*, *Powder Diffr.* **22** (2007) 130.
- [4] P. Palmer, S. Webber, K. Ferguson and R. Jacobs, *Use of field-portable XRF analyzers for rapid screening of toxic elements in FDA-regulated products*, *J. Agric. Food Chem.* **57** (2009) 2605.
- [5] Amptek Inc. webpage, <http://www.amptek.com/products/xr-100sdd-silicon-drift-detector/>.
- [6] M.N. Mazziotta, *Electron-hole pair creation energy and Fano factor temperature dependence in silicon*, *Nucl. Instrum. Meth.* **A 584** (2008) 436.
- [7] M.V. Fischetti, *Monte Carlo simulation of transport in technologically significant semiconductors of the diamond and Zinc-Blende structures-part I: homogeneous transport*, *IEEE Trans. Electron Dev.* **38** (1991) 634.
- [8] S. Adachi, *Properties of group-IV, III-V and II-VI semiconductors*, John Wiley and Sons Inc., New York U.S.A. (2009).
- [9] I. Kanno et al., *InSb cryogenic radiation detectors*, *Nucl. Instrum. Meth.* **A 568** (2006) 416.
- [10] Y. Sato, Y. Morita, T. Harai and I. Kanno, *Photopeak detection by an InSb radiation detector made of liquid phase epitaxially grown crystals*, *Nucl. Instrum. Meth.* **A 621** (2010) 383.
- [11] Y. Sato, Y. Morita and I. Kanno, *Performance estimation of InSb compound semiconductor detectors as a function of active area using alpha particles*, *Nucl. Instrum. Meth.* **A 737** (2014) 1.
- [12] A. Saynatjoki et al., *InAs pixel matrix detectors fabricated by diffusion of Zn in a metal-organic vapour-phase epitaxy reactor*, *Nucl. Instrum. Meth.* **A 563** (2006) 24.
- [13] Y. Yatsu et al., *Study of avalanche photodiodes for soft X-ray detection below 20 keV*, *Nucl. Instrum. Meth.* **A 564** (2006) 134.
- [14] J.E. Lees et al., *Development of high temperature AlGaAs avalanche diodes for soft X-ray photon counting*, *JHEP* **6** (2011) C12007.
- [15] R.B. Gomes et al., *GaAs/Al_{0.8}Ga_{0.2}As avalanche photodiodes for soft X-ray spectroscopy*, 2014 *JINST* **9** P03014.
- [16] C.H. Tan et al., *Avalanche gain and energy resolution of semiconductor X-ray detectors*, *IEEE Tans. Electron Dev.* **58** (2011) 1696.
- [17] R.B. Gomes et al, *InAs avalanche photodiodes for X-ray detection*, 2011 *JINST* **6** P12005.
- [18] A.R.J. Marshall et al., *Electron dominated impact ionization and avalanche gain characteristics in InAs photodiodes*, *Appl. Phys. Lett.* **93** (2008) 111107.
- [19] P.J. Ker et al., *Temperature dependence of leakage current in InAs avalanche photodiodes*, *IEEE J. Quantum Elect.* **47** (2011) 1123.